Eigenchannel quantum-defect theory of open-shell atoms. I. Autoionization resonances and eigenphase shifts of chlorine

Z.-w. Wang* and K. T. Lu†
Argonne National Laboratory, Argonne, Illinois 60439
(Received 5 March 1984)

A multichannel quantum-defect theory focused on the time-delay matrix is applied to the analysis of Rydberg levels and autoionization resonances of the chlorine atom. The analysis shows that recently observed photoionization cross sections above the $3p^4(^3P)$ threshold of the chlorine ion may be interpreted in terms of unresolved groups of resonances with three different total angular momenta J and approximately the same energy. Experimental data of Rydberg levels were used to determine the phase shift of the collisional eigenstate (quantum defect) and the time-delay matrix for the electron-ion scattering process. The LS coupling scheme is assumed for the electron + ion compound state. The channel interaction strengths and dipole matrix elements of even-parity states relevant to electron-ion collisional and recombination processes are obtained. The branching ratio of photoelectrons is calculated.

I. INTRODUCTION

The general relationship between the phase shift of electron-ion collisional wave functions and the quantum defect of discrete states is well known.[1] This relationship connects Rydberg states in the discrete spectrum with autoionization resonances in the continuum, and establishes a base for the channel notion of the multichannel quantum-defect theory (MQDT). Physical quantities in the discrete spectrum and in the continuum are expressed in terms of a single set of parameters.[2] Analytic expressions for the physical quantities consist mainly of trigonometric functions of effective quantum numbers ν_i, invariant under the transformation $\nu_i \rightarrow \nu_i + n$, n being an integer. This invariance accounts for the periodicity of the Rydberg series. These properties permit extraction of collisional information from the wealth of spectroscopic data. This method has been successful in analyzing Rydberg and autoionization spectra of closed-shell atoms, with ground-state total angular momentum $J_0 = 0$, such as noble-gas atoms.[2] For such atoms, one-electron ionization leads to simple ion structure, so that a two-ionization-limit-MQDT analysis is adequate. However, this approach has not been adapted for open-shell atoms, in which the spectra is complicated by the presence of numerous ion-core states. Channel interactions may occur among series converging to different ionization limits of the ion-core states. A further complication is caused by the nonzero ground-state total angular momentum J. By conventional continuum light sources,[3] photoexcitation and photoionization reaches two ($J_0 = \frac{1}{2}$) or three final states by dipole selection rules. These spectra with different J values overlap in the continuum. Open-shell atoms thus provide a challenging problem for theorists.[4,5]

In this paper we present a two-ionization-limit multichannel-quantum-defect treatment that introduces "effective channels" and time delay in disentangling the autoionization structures and determines partial photoionization cross sections between ionization limits $3p^4(^3P)$ and $3p^4(^1D)$ of the chlorine atom. Discrete Rydberg levels were analyzed and used as input to evaluate the eigenphase shifts and the diagonal elements of the time-delay matrix for the electron-ion scattering process. The effective channels and the related eigenphase shifts reduce the number of parameters in the theory and therefore simplify the problem greatly.

The calculations presented in this paper aim at demonstrating qualitative relationships and at correlating a wide range of experimental data. One limitation on accuracy should be explained at the outset. All quantum-defect parameters depend on the total energy of the system and their variations over an energy interval ΔE are of order $\Delta E/I$, where I is a specific ionization limit. The energy range ΔE over which the theory is of interest is a few times the separation of thresholds $I(^1D) - I(^3P)$, which is about $0.1I(^3P)$ for chlorine. Hence, the accuracy of the present calculation of autoionization cross sections between $3p^4(^1D)$ and $3p^4(^3P)$ ionization limits of the chlorine atom in neglecting the channel interactions with channels converging to the $3p^4(^1S)$ ionization limit is about 10%.

In Sec. II we develop a multichannel quantum-defect theory, focused on the time-delay matrix, which reduces a multichannel problem into a few pairs of interacting channels in analyzing the autoionization structures of open-shell atoms. In Sec. III we present the results for the chlorine atom. Finally, a conclusion is presented in Sec. IV.

II. THEORY: EFFECTIVE CHANNELS AND TIME DELAY

We deal with the motion of an electron in the Coulomb field surrounding an ionic core in terms of a collisional picture. We consider a set of discrete and continuum states of the complete system, ion plus electron, which

differ only in the energy of the excited electron and are specified by the orbital, spin, and fine-structure quantum numbers of the ion, the orbital and spin angular momentum of the electron, and the coupling of the electron to the ion core. For example, one-photon dipole absorption from the ground state of a chlorine atom, $3p^5\,^2P_{3/2}$, leads to 26 channels consisting of even-parity configurations $3p^4\epsilon l$ ($l=s$ or d) and $J=\frac{1}{2}$, $\frac{3}{2}$, and $\frac{5}{2}$, where ϵ is the orbital energy. There are seven channels belonging to $J=\frac{1}{2}$ [including five channels converging to $3p^4(^3P)$ states of the ion and two channels converging to the $3p^4(^1D_2)$ state of the ion], ten channels with $J=\frac{3}{2}$, and nine channels with $J=\frac{5}{2}$. There are also three channels converging to the $3p^4(^1S)$ ionization limit. The $3p^4(^1S)$ ionization limit lies about 2 eV above the $3p^4(^1D)$ ionization limit and there is no clear evidence of discrete levels or resonances converging to the $3p^4(^1S)$ ionization limit in the spectra range below the $3p^4(^1D)$ ionization limit. It is reasonable to neglect the channel interaction effect from channels converging to the $3p^4(^1S)$ ionization limit on the spectra lying below the $3p^4(^1D)$ ionization limit. As stated in the Introduction, the error generated amounts to about 10%. We thus adopt a two-ionization-limit model in analyzing autoionization structures between ionization limits $3p^4(^3P)$ and $3p^4(^1D)$. A complete list of the LS-coupled channels converging to the $3p^4(^3P)$ and $3p^4(^1D)$ ionization limits is shown in Table I.

When the total energy, $E=I+\epsilon$, falls below the ground-state energy I of the ion core, e.g., $3p^4(^3P_2)$, we have $\epsilon<0$ for all channels. The complete eigenvalue problem of the discrete spectra is described by the compatibility equation[2]

$$F(\nu_1,\ldots,\nu_k,\mu_\alpha,U_{i\alpha})=\det\,|\,U_{i\alpha}\sin[\pi(\nu_k+\mu_\alpha)]\,|\,=0\ , \tag{1}$$

where μ_α and $U_{i\alpha}$ are eigenvalues and eigenvectors of an R matrix that measures short-range non-Coulombic interactions between the electron and the ion core. The asymptotic wave function of the outer electron, from the scattering point of view, is far separated from the remaining ion core in configuration space; the electron is attached to the ion by the Coulomb field and forms a dissociation channel (i channel). This solution is a linear combination of two independent Coulomb wave functions and determines the regular energy spacings of successive levels of a series. The mixing coefficients of the wave function are determined by the normalization factor and by matching the boundary conditions at the ion core, where the electron and ion core form a compound-state channel (α channel). ν_k is the effective quantum number of the electron, related to its energy ϵ_k in atomic units by

$$\epsilon_{kn}=E_n-I_k=-\frac{1}{2\nu_{kn}^2}\ , \tag{2}$$

where I_k is the ionization potential. ν_{ln} is treated as a continuous varying function of energy, i.e., $\nu_{ln}=\nu_l(E)$. The quantum defect μ is identified as $\mu=\nu_l-n$, or $\mu=-\nu_l$ (mod 1).

In the autoionization region the total energy E lies between I_1 and I_2, where I_1 and I_2 are the threshold energies of ion-core levels $3p^4(^3P)$ and $3p^4(^1D)$, respectively. Here we neglect the small fine-structure splitting of the core state $3p^4(^3P)$. The ratio between the spin-orbit splitting energy and the total energy is $\sim 10^3/10^5$. It amounts to one percent accuracy for high-lying levels and several percent accuracy for low-lying levels in replacing $\nu_1\simeq\nu_a\simeq\nu_b\simeq\nu_c$, where ν_a, ν_b, and ν_c are the effective quantum numbers of the three fine-structure components of the core state $3p^4(^3P_{2,1,0})$, with threshold energies I_a, I_b, and I_c, respectively. In this energy range, $I_2>E>I_1\sim I_a\sim I_b\sim I_c$, 18 channels become open (denoted $k\in P$), and $\nu_k=i/k_k$ is imaginary and degenerate in energy, where eight channels remain closed (denoted $k\in Q$) and ν_k remains real (see Table I). The asymptotic behavior of wave functions in this region requires oscillatory standing waves in the open channels and exponentially damped waves in the closed channels. This can be achieved by introducing eigenstates ρ, such that each eigenstate ρ is a superposition of the standing waves of open channels with the same eigenphase shift[6] $\pi\tau_\rho$. An essential point of the present treatment is the establishment of the following relation, for $k\in P$:

$$\nu_1\leftrightarrow-\tau_p\ (\text{mod } 1)\ . \tag{3}$$

The compatibility condition which describes the eigenvalue problem in the autoionization region becomes

$$F(-\tau_\rho,\nu_2)=\det\,|\,U_{i\alpha}\sin[\pi(-\tau_\rho+\mu_\alpha)]\,|\,=0\ ,\qquad \rho\in P\ . \tag{4}$$

Equation (4) represents functional curves in a $(-\tau_\rho,\nu_2)$ plot. This means that the variable ν_1 of each level of the discrete spectrum can be represented in the form $\nu_1=n-\tau_\rho$, where $\pi\tau_\rho$ represents the phase shift of the collision eigenstate ψ_ρ for the autoionization region. This procedure allows one to use low-resolution discrete data by neglecting the fine-structure splitting, i.e., $\nu_1\simeq\nu_a\simeq\nu_b\simeq\nu_c$, to infer the collisional eigenphase shift graphically.

Figure 1(a) shows an example of a three-channel quantum-defect plot (μ,ν_2) constructed with $3p^4(^3P_2)$ and

TABLE I. The possible channels of the Cl atom ($J=\frac{1}{2}$, $\frac{3}{2}$, $\frac{5}{2}$, and even parity).

Configuration	$J=\frac{1}{2}$	$J=\frac{3}{2}$	$J=\frac{5}{2}$
$3p^4[^3P]ns$	^4P	^4P	^4P
	^2P	^2P	
$3p^4[^3P]nd$	^4D	^4F	^4F
	^4P	^4D	^2F
	^2P	^2D	^4D
		^4P	^2D
		^2P	^4P
$3p^4[^1D_2]ns$		^2D	^2D
$3p^4[^1D_2]nd$	^2P	^2D	^2F
	^2S	^2P	^2D

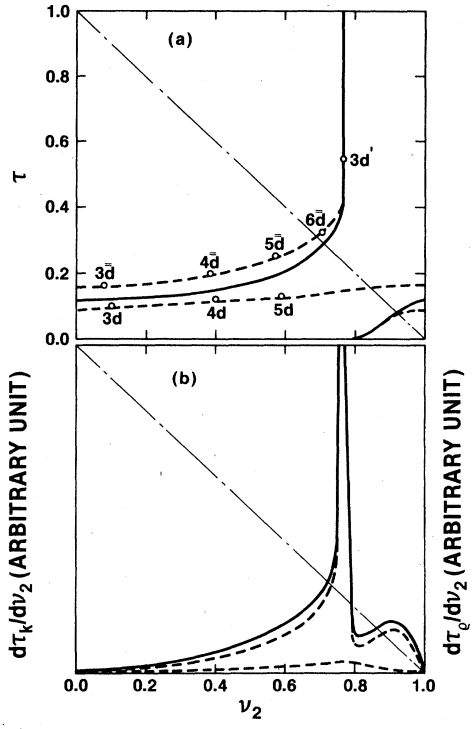

FIG. 1. (a) The (τ,ν_2) plots for $J=\frac{3}{2}$ in two alternative treatments. The dashed curves represent a three-channel problem with $3p^4(^3P)nd$, $3p^4(^3P)n\bar{d}$, and $3p^4(^1D)nd'\,^2P$ channels. The solid curves represent an effective two-channel problem with $3p^4(^3P)nd\,^2\bar{P}$ and $3p^4(^1D)nd'\,^2P$. (b) The relation of time-delay $d\tau_k/d\nu_2$ (represented by solid curves) with $d\tau_\rho/d\nu_2$ (represented by dashed curves).

$3p^4(^1D_2)$ as the first two ionization thresholds. The discrete energy levels are marked in the figure. The dashed curves represent the functional curves of Eq. (4), the $(-\tau_\rho,\nu_2)$ plot. The two horizontal curves represent the two open channels, $\epsilon\bar{d}$ and ϵd, while the vertical curve represents the closed channel. The avoided crossings indicate channel interactions. Since Eq. (4) contains trigonometric functions in τ_ρ and ν_2, the functional dependence of the $(-\tau_\rho,\nu_2)$ plot is doubly periodic, with period 1, in both τ_ρ and ν_2. This means that the dashed curves are connected in one curve in the unit square plot. For example, the upper and lower branches represent $\tau_\rho=\tau_1$ perturbed by the closed channel located at $\nu_2\simeq 0.77$. The middle branch represents τ_2 and interacts weakly with the closed channel. The τ_1 and τ_2 branches are connected to each other at $\nu_2=0.0$ and 1.0.

The periodic character of the eigenphase τ_ρ in the presence of the closed channels Q, as implied by Eq. (4), can be described by the following relation:[2]

$$\sum_\rho \tau_\rho(\nu_2+1)=q+\sum_\rho \tau_\rho(\nu_2)\ . \tag{5}$$

It states that the total accumulated phase shift $\tau(\nu_2)=\sum_\rho \tau_\rho(\nu_2)$ of all the open channels increases by an integer q, where q is the total number of closed channels, as ν_2 increases by one unit. The dashed curves in Fig. 1 correspond to the situation in Eq. (5) with two open channels, $\rho=1$ and 2, and one closed channel, $q=1$. Equations (4) and (5) describe the behaviors of perturbations of eigenphases as well as quantum defects near resonances, and they are connected by Eq. (3). In this regard, Eqs. (4) and (5) are a generalization of Macek's treatment on the behaviors of eigenphases near a resonance.[7]

The slope of the eigenphase τ_ρ, $d\tau_\rho/d\nu_2$, is proportional to the diagonal element of the time-delay matrix.[8,9] It measures the channel interaction strength between each open channel and all the closed channels.

From Eq. (5) we obtain

$$\sum_\rho d\tau_\rho(\nu_2)/d\nu_2=d\tau_k(\nu_2)/d\nu_2\ . \tag{6}$$

This relation shows that the channel interaction strength of the total phase shift of all open channels, $\tau_k=\sum_\rho \tau_\rho(\nu_2)$, with closed channels is equal to the sum of the partial channel interaction strength of each open channel with all the closed channels. This quantity, $d\tau_k(\nu_2)/d\nu_2$, is proportional to "time delay," which is the trace of the time-delay matrix.[9] This relation implies that one could replace the effect due to a closed channel on multiopen channels by a *single* effective open channel without loss of generality.

Figure 1(a) shows the relationship of (τ,ν_2) plot for a three-channel problem, $3p^4(^3P)nd$, $3p^4(^3P)n\bar{d}$, and $3p^4(^1D)nd'\,^2P$, with an effective two-channel problem, $3p^4(^3P)nd\,^2\bar{P}$ and $3p^4(^1D)nd'\,^2P$ (represented by solid curves). Figure 1(b) shows the relationship of time-delay

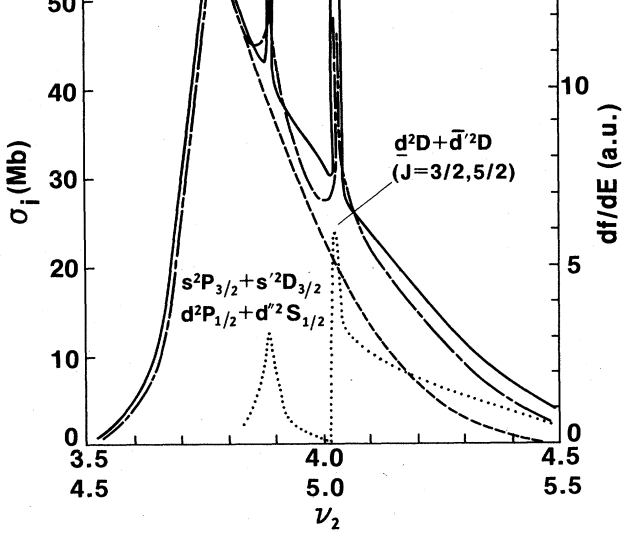

FIG. 2. Chlorine photoionization cross section between $3p^4(^3P)$ and $3p^4(^1D)$ thresholds. The solid curve represents the measured values by Ruščić *et al.* (Ref. 3) plotted as a function of ν_2. The dashed and dotted curves are the results obtained by six pairs of two-channel fittings. The dot-dashed curve represents the total photoionization cross section, i.e., the sum of all six partial cross sections.

$d\tau_k/d\nu_2$ with $d\tau_\rho/d\nu_2$. The effective phase shift (solid curve) is obtained by averaging the eigenphase shifts of the $n\bar{d}$ and nd channels, τ_1 and τ_2, so that the slope of the solid curves equals that of the sum of the dashed curves in Fig. 1(a) as required by Eq. (6), as shown in Fig. 1(b). The validity of the eigenphase shift relation (5) and the channel-interaction-strength relation (6) relies on the *independence* in energy of quantum-defect parameters μ_α and $U_{i\alpha}$, since the energy dependence of the parameters breaks the *periodicity* of the functional dependence of τ and ν_2. Following this procedure, the photoionization cross section can be expressed as a superposition of pairs of two-channel formulas:

$$df^{(J)}(\nu_2)/dE=\sum_\rho df^{(\rho,J)}(\nu_2)/dE$$
$$=2(E-E_0)\left[\left[\sum_k I_k\sin^2[\pi(\nu_2-\nu_k)](d\tau_k/d\nu_2)\right]_J+I_{0J}\right], \quad (7)$$

where I_{0J} represents the continuum background intensity and the slope $d\tau_k/d\nu_2$ measures the channel interaction strength between the effective open channel and the kth closed channel. The effective eigenphase shift τ_k represents the result of prediagonalization[10] of all open channels on the wave function of the kth closed channel.

For the two-channel case the density of the oscillator strength of an autoionization resonance can be written as[11]

$$df(\nu_2)/dE=2(E-E_0)I_k\sin^2[\pi(\nu_2-\nu_k)](d\tau_k/d\nu_2) \quad (8)$$

and

$$I_k=\frac{D_1^2\cos^2\theta+D_2^2\sin^2\theta+2D_1D_2\sin\theta\cos\theta\cos[\pi(\mu_1-\mu_2)]}{\sin^2\theta\cos^2\theta\sin^2[\pi(\mu_1-\mu_2)]}, \quad (9)$$

where θ is the mixing angle, E_0 is the energy of the ground state, D_α ($\alpha=1,2$) are the dipole matrix elements, and ν_0 represents the value of ν_2 at which df/dE vanishes. The addition of the continuum background intensity I_{0J} in Eq. (7) guarantees[12] conservation of flux below and above the ionization limit $3p^4(^3P)$. A detailed derivation of this key result in Eq. (7) will be published elsewhere.

III. RESULTS AND DISCUSSION

We make use of the relationship Eq. (3) between discrete energy levels and continuum eigenstates to construct the eigenphase shift τ_ρ of the electron-ion collisional process from discrete experimental data.[13] Three sets of the quantum-defect plot (μ,ν_2) corresponding to three J values ($=\frac{1}{2}$, $\frac{3}{2}$, and $\frac{5}{2}$) were constructed with $3p^4(^3P_2)$ and $3p^4(^1D_2)$ as the first two ionization thresholds.[14] These plots show the correspondence between bound-state levels in terms of quantum-defect μ and eigenphases τ_ρ in the autoionization region, a correspondence which is expressed by Eq. (3). From these results we locate the position of resonances belonging to closed channels in the ν_2 scale and their corresponding interacting open channels. For example, the broad resonance seen in the photoionization cross-section data,[3] replotted on the ν_2 scale in Fig. 2, results from the interactions between closed channels $3p^4(^1D)nd'\,^2P$ with $J=\frac{1}{2}$ and $\frac{3}{2}$ and their corresponding open channels.

It is worthwhile to note that two autoionization cross sections have been replotted on the ν_2 scale (from 3.5 to 5.5) and the results are within 2% agreement. This illustrates the periodicity of the autoionization resonances in the ν_2 scale and justifies the assumption of energy-independent quantum-defect parameters. The sharp peak at $\nu_2=4.03$ is due to the interactions between closed $3p^4(^1D)n\bar{d}'\,^2D$ and open channel $3p^4(^3P)\epsilon\underline{d}\,^2D$ with $J=\frac{3}{2}$ and $\frac{5}{2}$, respectively. The other sharp peak at $\nu_2=3.89$ is due to the interactions of closed channels $3p^4(^1D)nd''\,^2S_{1/2}$ and $3p^4(^1D)ns'\,^2D_{3/2}$ with open channels. We can reduce the full multichannel problem to a two-channel problem by introducing effective channels according to Eqs. (5) and (6). The upper part of Fig. 3 shows the six sets of the (τ,ν_2) plot obtained from discrete energy levels. The solid curves in the figure are fitted results of $F(\tau,\nu_2)=0$ following the standard fitting procedures of MQDT.[6] The basic quantum-defect parameters, i.e., μ_α and mixing angle θ for these six pairs of two-channel problems obtained, are listed in Table II.

The values of D_α are determined from Eq. (7)—(9) by comparing with photoionization cross-section data[3] in Fig. 2. The final values of D_α are also listed in Table II. The values of partial df/dE for each pair of the effective two-channel problem are plotted in the lower part of Fig. 3. The values of partial cross sections resulting from the

TABLE II. MQDT parameters.

Channel	μ_α	θ	D_α^2 (a.u.)
$3p^4(^3P)nd\,^2\bar{F}_{1/2,3/2}$	0.31	50.33°	1.01
$3p^4(^1D)nd'\,^2P_{1/2,3/2}$	0.09		2.35
$3p^4(^3P)n\underline{d}\,^2D_{3/2,5/2}$	0.16	22.2°	4.24
$3p^4(^1D)n\bar{d}'\,^2D_{3/2,5/2}$	0.97		0.72
$3p^4(^3P)nd\,^2P_{1/2}$	0.24	40.2°	0.3
$3p^4(^1D)nd''\,^2S_{1/2}$	0.04		0.028
$3p^4(^3P)ns\,^2P_{3/2}$	0.13	37.1°	0.36
$3p^4(^1D)ns'\,^2D_{3/2}$	0.05		0.145

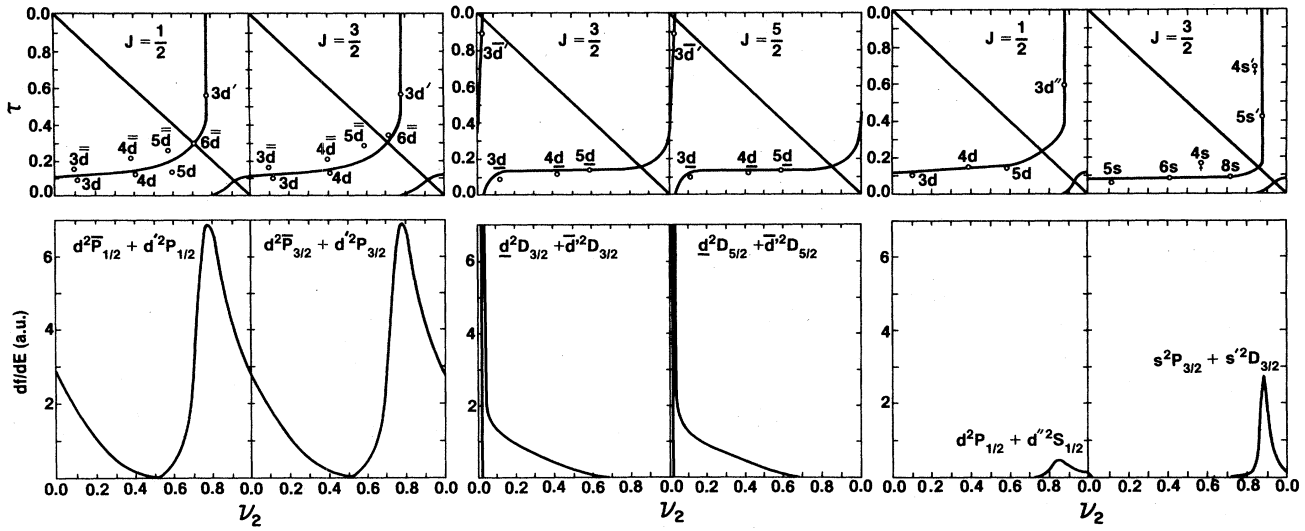

FIG. 3. Eigenphases τ and oscillator strength densities for six pairs of two-channel problems. The upper part shows the six sets of (τ,ν_2) plots. The lower part represents the values of partial df/dE for each pair of two-channel problems.

interactions between the effective channel $3p^4(^3P)nd\,^2\bar{P}$ $[=3p^4(^3P)nd+3p^4(^3P)n\bar{d}]$ and $3p^4(^1D)nd'\,^2P$ ($J=\frac{1}{2}$ and $\frac{3}{2}$) reproduces the major features of the experimental data as shown by dashed curves in Fig. 2. One sharp peak located at $\nu_2=4.03$ arises from the interactions of $3p^4(^3P)\underline{d}\,^2D$ with $3p^4(^1D)\bar{d}'\,^2D$ ($J=\frac{3}{2}$ and $\frac{5}{2}$). The other peak located at $\nu_2=3.89$ arises from the interactions of $3p^4(^3P)ns\,^2P_{3/2}$ with $3p^4(^1D)ns'\,^2D_{3/2}$ and the interactions of $3p^4(^3P)nd\,^2P_{1/2}$ with $3p^4(^1D)nd''\,^2S_{1/2}$. The partial cross sections due to these two sharp resonances are represented by dotted curves in Fig. 2. The total photoionization cross section corresponds to the sum of all these six partial cross sections and the results are plotted in Fig. 2 by the dot-dashed curves. The agreement with experiment is satisfactory.

In the energy range $E>I_2$ the branching ratio of the two groups of photoelectrons can be written as[6]

$$\frac{df_1}{dE}\Big/\frac{df_2}{dE}=\frac{\sum_{i\in P}\sum_{\alpha,\beta}U^{+}_{\alpha i}U_{i\beta}\cos[\pi(\mu_\alpha-\mu_\beta)]D_\alpha D_\beta}{\sum_{i\in Q}\sum_{\alpha,\beta}U^{+}_{\alpha i}U_{i\beta}\cos[\pi(\mu_\alpha-\mu_\beta)]D_\alpha D_\beta}\,. \tag{10}$$

Using the value of the parameters shown in Table II, we obtain $[(df/dE)(^3P)]/[(df/dE)(^1D)]=1.7$. The experimental result[15] at 21.2 eV is 1.85.

IV. CONCLUSION

We have obtained eigenphase shifts and partial photoionization cross sections of the chlorine atom based on the introduction of effective channels. We have reduced a 26-channel problem to six pairs of interacting channels and the number of parameters from 154 to 20. The behavior of eigenphase shifts near resonances, the continuity of channel interactions, and the conservation of flux across the thresholds are all treated properly through the analytic relations in Eqs. (5)—(7), respectively. This simple and reliable method can be used to calculate, on the basis of discrete spectroscopic and low-resolution photoionization data, excitation cross sections for electron-ion collision processes[16] near threshold and dielectronic-recombination processes,[1] where resonance phenomena precede relaxation mechanisms such as autoionization or predissociation.

ACKNOWLEDGMENTS

This work has been performed under the auspices of the U.S. Department of Energy. One of us (Z.-w.W.) was a Visiting Foreign Scholar at Argonne National Laboratory. We acknowledge Dr. M. Inokuti for a critical reading of this manuscript and Professor U. Fano for constructive comments.

*Permanent address: Institute of Atomic and Molecular Physics, Jilin University, Changchun, People's Republic of China.

†Present address: Graduate School, Academia Sinica, Beijing, People's Republic of China.

[1]M. J. Seaton, Rep. Prog. Phys. **46**, 167 (1983), and references therein.

[2]K. T. Lu, in *Photophysics and Photochemistry in Vacuum Ultraviolet,* edited by S. P. McGlynn, G. L. Findley, and R. H. Huebner (Reidel, Dortrecht, Holland, 1983); U. Fano, J. Opt. Soc. Am. **65**, 979 (1975).

[3]B. Ruščić and J. Berkowitz, Phys. Rev. Lett. **50**, 675 (1983).

[4]M. Lamoureux and F. Combet-Farnoux, J. Phys. (Paris) **40**, 545 (1979).

[5]E. R. Brown, S. L. Carter, and H. P. Kelly, Phys. Rev. A **21**, 1237 (1980).

[6]K. T. Lu, Phys. Rev. A **4**, 579 (1971).

[7]J. Macek, Phys. Rev. A **2**, 1101 (1970).
[8]K. T. Lu and A. R. P. Rau, Phys. Rev. A **28**, 2623 (1983), and references therein; A. Giusti-Suzor and U. Fano, J. Phys. B **17**, 215 (1984).
[9]F. T. Smith, Phys. Rev. **118**, 349 (1960).
[10]U. Fano, Phys. Rev. **124**, 1866 (1961), Sec. IV.
[11]K. T. Lu, Proc. R. Soc. London, Ser. A **353**, 431 (1977).
[12]M. Gailitis, Zh. Eksp. Teor. Fiz. **44**, 1974 (1963) [Sov. Phys.—JETP **17**, 1328 (1963)].
[13]L. J. Radziemski, Jr. and V. Kaufman, J. Opt. Soc. Am. **59**, 424 (1969).
[14]Z.-w. Wang, R.-G. Wang, and K. T. Lu, Abstract, p. 80, Symposium on Atomic Spectroscopy, Lawrence Berkeley Laboratory Report No. LBL-16509, 1983 (unpublished).
[15]J. Berkowitz, C. H. Batson, and G. L. Goodman, Phys. Rev. A **24**, 149 (1981).
[16]Li Jia-ming (C.M.Lee), Acta Phys. Sin. **29**, 419 (1980).